Available online at www.sciencedirect.com

ScienceDirect

Nuclear and Particle Physics Proceedings 267–269 (2015) 207–216

www.elsevier.com/locate/nppp

High-energy QCD: Interplay of nonperturbative and perturbative effects

B. Z. Kopeliovich[a,b]

(a) Departamento de Física, Universidad Técnica Federico Santa María;
(b) Centro Científico-Tecnológico de Valparaíso
Avda. España 1680, Casilla 110-V, Valparaíso, Chile

Abstract

Soft interaction is an unavoidable participant of every hard process at high energies. Although the factorisation theorems allow to separate the hard and soft parts of the interaction, in many instances (not covered by the theorems) factorisation is broken, and the processes are dominated by the interplay between the perturbative and nonperturbative effects. Several examples are overviewed in this note.

Keywords: QCD, Perturbative QCD, Nonperturbative QCD, Factorization, Diffraction

1. Introduction

Most of hadronic reactions involve nonperturbative effects, even if they are characterized by a hard scale. In the classical example of deep-inelastic lepton scattering (DIS) on a proton, the soft scale is essentially involved even at large momentum transfer Q, as is illustrated in Fig. 1. The powerful tool, which allows to separate the perturbative and nonperturbative part of the interaction is QCD factorisation theorems (sometimes not proven) [1]. However, in many instances the hard and soft interactions are not separable, and their interplay is crucial for theoretical interpretation of the processes. In what follows we briefly overview several effects breaking factorisation.

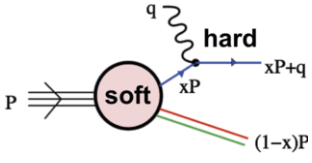

Figure 1: Inclusive Deep-Inelastic Scattering of leptons on protons.

According to Bjorken scaling the parton distributions in a hadron depend only on x, the fractional momentum of the parton. This could be true if the number of partons were conserved. However, they are not classical particles, but quantum fluctuations, whose number depends on reference frame and resolution Q of the probe.

A photon of virtuality Q^2 can resolve partons with transverse momenta $k_T < Q$, but it is blind to harder fluctuations. Increasing Q^2, one can see more partons in the proton, because a feed-down mechanism from large x partons populates the small-x region. Simultaneously this leads to a reduction of the parton density at large x. Such a re-distribution of parton momenta leads to a Q^2-dependence falling at large and rising at small x. Such a peculiar behaviour is confirmed by DIS data [6].

Perturbative QCD is unable to predict the parton distribution functions (PDF), because of the presence of the nonperturbative effects. However, one can calculate how PDFs vary with hard scale. The scale evolution is controlled by the DGLAP equations (Dokshitzer-Gribov-Lipatov-Altarelli-Parisi) [2, 3, 4, 5],

$$Q^2\frac{d}{dQ^2}\begin{pmatrix} q_f(x,Q^2) \\ g(x,Q^2)\end{pmatrix} = \frac{\alpha_s}{2\pi}\int_x^1 \frac{dx_1}{x_1} \times \begin{pmatrix} P_{ff}\left(\frac{x}{x_1}\right) & P_{fg}\left(\frac{x}{x_1}\right) \\ P_{gf}\left(\frac{x}{x_1}\right) & P_{gg}\left(\frac{x}{x_1}\right)\end{pmatrix}\begin{pmatrix} q_f(x_1,Q^2) \\ g(x_1,Q^2)\end{pmatrix} \quad (1)$$

http://dx.doi.org/10.1016/j.nuclphysbps.2015.10.104

The splitting functions $P_{ij}(x)$ for transition between the parton species $i \to j$ are calculated perturbatively. Therefore, the usual strategy for extracting PDFs from DIS data is: (i) introduce an ad hoc PDF parametrization at some starting scale Q_0^2; (ii) evolve it with DGLAP evolution to higher scales; (iii) compare with data at a proper scale and adjust the input PDFs.

2. Drell-Yan reaction

The Drell-Yan reaction of heavy dilepton production in hadronic collisions, $h_1h_2 \to l^+l^-X$, can be represented as annihilation of the projectile quark and antiquark originated from the colliding hadrons, as is illustrated in Fig. 2.

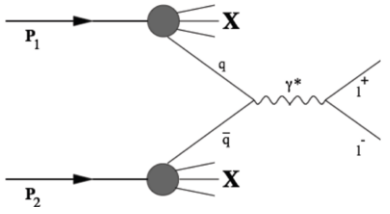

Figure 2: Drell-Yan mechanism for production of a heavy dilepton (leading order).

The cross section reads [7],

$$\frac{d\sigma}{dM^2} = \int_0^1 dx_1 dx_2 \sum_f \frac{d\hat{\sigma}(q_f\bar{q}_f \to \bar{l}l)}{dM^2} \times \Big\{q_f(x_1, M^2)\bar{q}_f(x_2, M^2) + (1 \leftrightarrow 2)\Big\}, \qquad (2)$$

where

$$\frac{d\hat{\sigma}(q_f\bar{q}_f \to \bar{l}l)}{dM^2} = \frac{4\pi\alpha_{em}^2 Z_f^2}{3N_c M^2}\,\delta(x_1x_2\,s - M^2), \qquad (3)$$

and the fractional momenta of the colliding q_f-$\bar{q}_f$ are related to the invariant mass and Feynman x_F of the dilepton $\bar{l}l$ as, $x_1x_2 = M^2/s$ and $x_1 - x_2 = x_F$.

The key result of the factorisation theorem, universality of $q_f(x, M^2)$, allows to predict the cross section Eq. (2). However, this leading order (LO) prediction dramatically underestimates data by a factor $K \approx 2.3$. *Why*?

Any abrupt variation of a current (electromagnetic or coloured) leads to an intensive radiation. In particular, this happens in the hard sub-process $q\bar{q} \to l\bar{l}$. Indeed, the colliding quarks carry a colour field of Weizäcker-Williams gluons, which are shaken off the colour sources, q and $\bar{q}$, when they disappear. The probability of no radiation in such a process is Sudakov suppressed and is small. Not a surprise that the cross section of the process depicted in Fig. 2, which is calculated in LO in α_s, so does not include gluon radiation, is suppressed compared with data. Indeed, the next to leading (NLO) order corrections improve agreement with data (see comparison with data in [8]).

3. Alternative dipole description: small-x DIS

At high energies, or small $x = Q^2/W^2 \ll 1$ the parton model description of DIS (and any other process) is not Lorentz invariant, only observables are. One cannot even say whether a sea parton belongs to the beam or target. The proton structure function $F_2(x, Q^2)$ at small x in the proton rest frame looks more like the hadronic structure of the virtual photon, like is illustrated in Fig. 3. The whole process is interpreted as

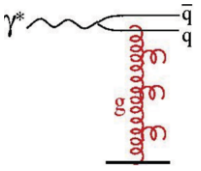

Figure 3: DIS in the proton rest frame.

interaction of a hadronic fluctuation of the incoming photon, containing a $\bar{q}q$ and accompanied gluons, and sea quarks. Important is the hierarchy of the fluctuation lifetimes: $t(l \to l'\gamma^*) \gg t(\gamma^* \to \bar{q}q) \gg t(\bar{q}q \to \bar{q}qg) \gg t(g \to gg)$, etc.

The distribution amplitude $\Psi^{T,L}_{q\bar{q}}(\alpha, r_T)$ of the transition $\gamma^* \to \bar{q}q$, illustrated in Fig. 4, is characterised by the transverse $\bar{q}q$ separation r_T and the fractional light-cone quark momentum α. Correspondingly, the inclu-

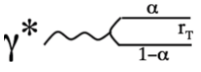

Figure 4: The transition amplitude of $\gamma^* \to \bar{q}q$.

sive $\gamma^* p$ cross section has the form,

$$\sigma_{\gamma^* p}(x, Q^2) = \sigma_T + \sigma_L = \frac{4\pi^2\alpha_{em}}{Q^2}\,F_2(x, Q^2), \qquad (4)$$

where the cross sections of transversely and longitudinally polarised photons can be calculated in the dipole approach [9] as [10],

$$\sigma^{\gamma^* p}_{T,L} = \int_0^1 d\alpha \int d^2r_T \left|\Psi^{T,L}_{q\bar{q}}(\alpha, r_T)\right|^2 \sigma_{q\bar{q}}(r_T) \qquad (5)$$

This dipole representation is based on another kind of factorisation: the dipole distribution function vs dipole cross section.

Perturbatively $\sigma_{\bar{q}q}(r_T)$ would be universal and flavour independent [9], what allows to predict various hard reactions. No sizeable deviation from this expectation caused by non-perturbative effects has been observed so far.

The light-cone distribution function $\left|\Psi^{T,L}_{q\bar{q}}(\alpha, r_T)\right|^2$ can be calculated perturbatively [11, 12].

$$\left|\Psi^{T}_{q\bar{q}}(\alpha, r_T)\right|^2 = \frac{2N_c\alpha_{em}}{(2\pi)^2}\sum_{f=1}^{N_f} Z_f^2\Big\{[1-2\alpha(1-\alpha)] \times \epsilon^2 \mathrm{K}_1^2(\epsilon r_T) + m_f^2 \mathrm{K}_0^2(\epsilon r_T)\Big\} \quad (6)$$

$$\left|\Psi^{L}_{q\bar{q}}(\alpha, r_T)\right|^2 = \frac{8N_c\alpha_{em}}{(2\pi)^2} \times \sum_{f=1}^{N_f} Z_f^2 Q^2\alpha^2(1-\alpha)^2 \mathrm{K}_0^2(\epsilon r_T) \quad (7)$$

Here $\alpha = p_q^+/p_{\gamma^*}^+$; $\epsilon^2 - \alpha(1-\alpha)Q^2 + m_f^2$. The mean dipole separation is $\langle r_T\rangle \sim 1/\epsilon$. Even at a large scale Q^2 in asymmetric fluctuations, called aligned jet configurations, when either $\alpha \sim 1/Q^2$, or $1-\alpha \sim 1/Q^2$, the large term in ϵ is compensated, and $\epsilon \sim m_f$, i.e. $\langle r_T\rangle$ is large and the fluctuation becomes soft.

The dipole cross section has the property of colour transparency [9]. If the mean dipole size is $\langle r_T\rangle \sim 1/Q$, the cross section is decreasing as $1/Q^2$. Otherwise the aligned jet configurations having a large cross section, are suppressed by their phase-space weight, which is also $\sim 1/Q^2$. Thus, the cross section Eq. (4) is falling with the scale as $1/Q^2$, which was anticipated according to Bjorken scaling.

4. Diffractive DIS

Diffractive interaction, which is associated with presence of a large rapidity gap in final state, in the case of DIS looks like excitation of the virtual photon $\gamma^* + p \to X + p$, with the state X having invariant mass $M_X \ll W$, as is illustrated in Fig. 5. Production of a rapidity gap is a result of a colourless exchange, which is dominated by the Pomeron, if the gap is large.

In the dipole representation, this process looks like a transition $\gamma^* \to \bar{q}q$ followed by elastic dipole-proton scattering via Pomeron exchange. Since the

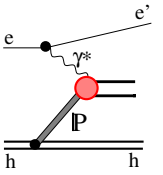

Figure 5: Diffractive DIS $\gamma^* + h \to X + h$ via Pomeron exchange.

forward elastic and total cross sections are related as $d\sigma_{el}/dt|_{t=0} = \sigma^2_{tot}/16\pi$, the single-diffraction cross section looks similar to the inclusive one, Eq. (5), but the dipole cross section is squared,

$$\int dM_X^2 \left.\frac{d\sigma^{DIS}_{sd}}{dM_X^2 dt}\right|_{t=0} = \frac{1}{16\pi}\int d^2 r_T\, \sigma^2_{q\bar{q}}(r_T) \times \int_0^1 d\alpha \left|\Psi_{q\bar{q}}(\alpha, r_T, Q^2)\right|^2 \quad (8)$$

Here $X = q + \bar{q}$, which corresponds to the PPR term in the triple-Regge phenomenology, as is illustrated in Fig. 6. The triple-Pomeron term PPP corresponds to excitation of a higher component of the photon, containing gluons, $X = q + \bar{q} + g$.

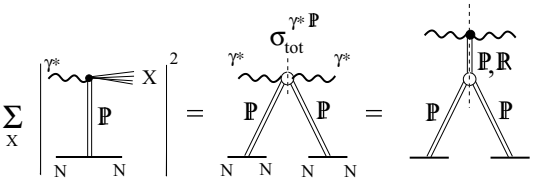

Figure 6: Triple-Regge description of diffractive DIS.

Usually diffraction in hadronic collisions is considered as a soft process [13], however in DIS it is characterised with a hard scale Q^2. *Is DIS diffraction hard or soft?*

As was explained in the previous sections, most of fluctuations of a highly virtual photon are hard, i.e. the $\bar{q}q$ dipole has a small size $\sim 1/Q$. Only a tiny fractions, whose probability is suppressed as $\sim 1/Q^2$, are soft, i.e. have a large hadronic size. The interplay between the probabilities and cross sections of hard and soft fluctuations of a highly virtual transverse photon can be viewed as it is presented in a simplified form in Table 1 [14].

From this simple representation for the Q-dependent parts of the cross sections we can conclude: (i) Inclusive DIS is semi-hard, semi-soft even at high Q^2; (ii) The fractional contribution of soft interactions is nearly Q^2-independent, $\sigma^{DIS}_{diff}/\sigma^{DIS}_{incl} \approx Const$; (iii) DIS diffraction is soft-dominated.

Table 1: Interplay between the probabilities and cross sections of fluctuations of virtual photon.

	$\lvert C_\alpha\rvert^2$	σ_α	$\sigma_{tot} = \sum_{\alpha=soft}^{hard} \lvert C_\alpha\rvert^2\sigma_\alpha$	$\sigma_{sd} = \sum_{\alpha=soft}^{hard} \lvert C_\alpha\rvert^2\sigma_\alpha^2$
Hard	~ 1	$\sim \frac{1}{Q^2}$	$\sim \frac{1}{Q^2}$	$\sim \frac{1}{Q^4}$
Soft	$\sim \frac{m_q^2}{Q^2}$	$\sim \frac{1}{m_q^2}$	$\sim \frac{1}{Q^2}$	$\sim \frac{1}{m_q^2 Q^2}$

Notice that this presentation was intentionally simplified, in order to clarify the main issue, relative importance of hard and soft interactions. However, this simple picture misses log Q^2 terms.

5. Drell-Yan via dipoles

In the rest frame of the target the Drell-Yan (DY) reaction is interpreted differently from the parton model (see Fig. 2). It looks like radiation of a heavy photon (or Z, W) decaying into a dilepton. The DY amplitude expressed in terms of Feynman graphs is depicted in Fig. 7. In spite of absence of dipoles in this graphs, the

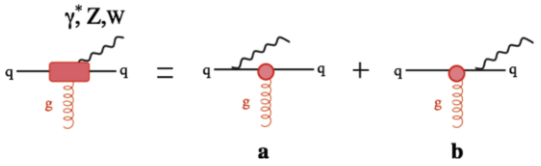

Figure 7: Bremsstrahlung of a heavy photon by a high-energy quark, before (a) and after (b) the interaction.

DY cross section can be expressed via the dipole cross section [15, 16],

$$\frac{d\sigma_{inc}^{(qp\to\gamma^* q' X)}}{d\alpha} = \int d^2r \left|\Psi_{q\gamma^*}(\vec{r},\alpha)\right|^2 \sigma_{\bar{q}q}(\alpha r, x_2)\,, \quad (9)$$

where $\Psi_{q\gamma^*}(\vec{r},\alpha)$ is the light-cone distribution function of the $|q\gamma^*\rangle$ component, which looks similar to Eqs. (6)-(7), and the explicit expressions can be found in [15, 17].

This nontrivial result can be understood intuitively as a result of interaction of different Fock components of the quark, namely, the bare quark $|q\rangle$ and $|q\gamma^*\rangle$. According to the basic principles of diffraction [18, 19, 20], if different Fock components interacted with the same cross section, no diffractive excitation would be possible, because the initial wave packet would be reproduced after the interaction. So diffraction emerges due to the difference between the interaction amplitudes of different components. While γ^* does not interact, the quark does, but it gets a relative shift of its impact parameter after radiation of the photon. Thus, one arrives at the difference of the quark-proton amplitudes with different impact parameters, which is equivalent to the dipole cross section [15]. This leads to Eq. (9).

The DY cross section, in a collision of two hadrons reads [17],

$$\frac{d\sigma_{inc}^{DY}}{dx_1 dM^2} = \frac{1}{M^2\, x_1}\,\frac{\alpha_{em}^2}{3\pi}\int_{x_1}^{1}\frac{d\alpha}{\alpha}\,F_2(x_1/\alpha) \times \int d^2r \left|\Psi_{q\gamma^*}^{L,T}(\vec{r},\alpha)\right|^2 \sigma_{\bar{q}q}(\alpha r, x_2)\,. \quad (10)$$

Here $F_2(x, M^2)$ is the structure function of the beam hadron, measured in DIS.

This simple formula reproduces the results of much more complicated NLO calculations at small $x < 0.01$ amazingly well. The comparison is presented in Fig. 8.

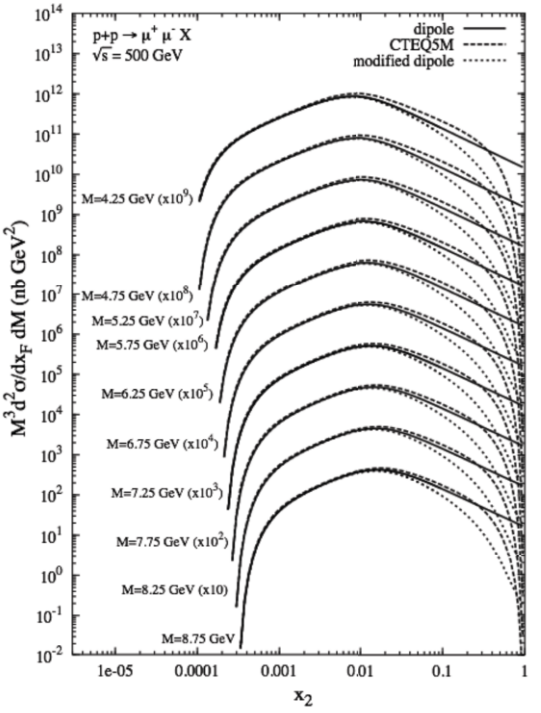

Figure 8: Comparison of the dipole approach, Eq. (10) (solid curve) with parton model NLO calculations using CTEQ5M parametrization (dashed curve) [8].

6. Diffractive Drell-Yan

Fig. 2 gives a hint of a possibility to measure in DIS the Pomeron structure function, which can be applied to other hard diffractive processes, assuming diffractive factorisation [21], which however, turns out to be broken, as is demonstrated further on in this and in the following section.

The Feynman graphs responsible for diffractive photon bremsstrahlung by a quark are depicted in Fig. 9. It

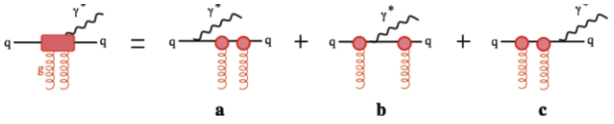

Figure 9: Feynman graphs for diffractive photon radiation.

turns out that radiation from the short line between the two exchanged gluons does not contribute, only external legs radiate [22]. This is actually a manifestation of the Landau-Pomeranchuk principle. For this reason, diffractive radiation of a photon (or any gauge boson) by a quark vanishes in the forward direction,

$$\left.\frac{d\sigma^{DY}_{inc}(qp\to\gamma^* qp)}{d\alpha\, dM^2 d^2p_T}\right|_{p_T=0} = 0. \qquad (11)$$

This can also be understood intuitively: since the photon does not interact, radiation occurs only due to the difference between impact parameters of the incident and recoil quarks. However the forward diffractive amplitude comes from the integral over impact parameter, so this difference cancels. This conclusion holds for any Abelian diffractive radiation of γ, W, Z bosons, Higgs.

Diffractive DIS, as it was demonstrated above, is dominated by soft interactions. On the contrary, diffractive Drell-Yan gets the main contribution from the interplay of soft and hard scales [23, 24]. Indeed, the quark radiating a heavy photon gets a shift in its location by $r \sim 1/M$. Correspondingly, the diffractive amplitude has the structure,

$$\sigma(\vec{R}) - \sigma(\vec{R} - \alpha\vec{r}) \;\propto\; \vec{r}\cdot\vec{R} \qquad (12)$$

This diffractive amplitude is not quadratic in r, like in inclusive DIS, but linear. Therefore, the soft part of the interaction is not enhanced in Drell-Yan diffraction, like was shown for diffractive DIS in Table 1, but it is semihard - semisoft, like inclusive DIS.

Such a structure of the diffractive amplitude includes all absorptive corrections (gap survival amplitude), provided that the dipole cross section is adjusted to data [24].

The Good-Walker form of the diffractive amplitude and the saturated shape of the dipole cross section, $\sigma(R) \propto 1 - \exp(-R^2/R_0^2)$, lead to unusual features of diffractive Drell-Yan,

$$\frac{\sigma^{DY}_{sd}}{\sigma^{DY}_{incl}} \propto \frac{\exp(-2R^2/R_0^2)}{R_0^2}, \qquad (13)$$

which can be seeing in Fig. 10. The fractional diffractive cross section is steeply falling with energy, but rises with the dilepton invariant mass, because the saturation scale $Q_s = 1/R_0$ in the dipole cross section rises with energy.

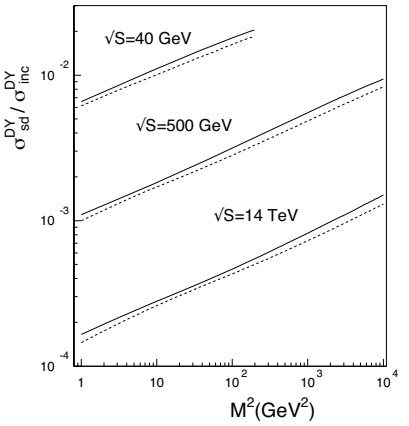

Figure 10: Fractional diffractive DY cross section as function of M^2 at different colliding energies.

Diffractive radiation of any Abelian particle is described by the same Feynman graphs, only couplings and spin structure may vary. Predictions for the dilepton invariant mass distributions at the LHC energy are shown in Fig. 11 for decays of different gauge bosons [25]. One can also compare with available data at

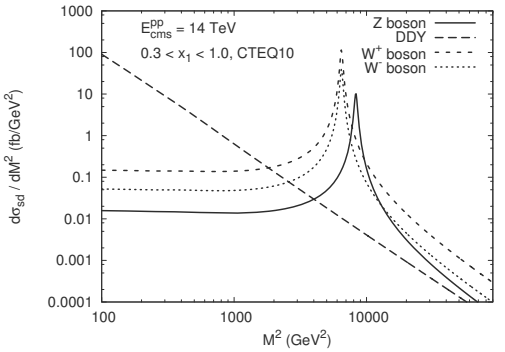

Figure 11: Diffractive cross section of gauge boson production at $\sqrt{s}$ = 14 TeV as function of dilepton invariant mass squared [25].

$\sqrt{s} = 1.96$ TeV from the CDF experiment [26], depicted

in Fig. 12. The parameter-free calculations performed

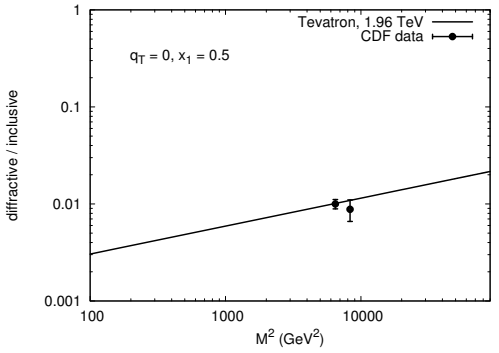

Figure 12: The fractional diffractive cross section as function of dilepton invariant mass squared. The CDF data points for W and Z production at $\sqrt{s} = 1.96$ TeV [26].

in the dipole approach agree with data quite well.

7. Diffractive excitation of heavy flavours

The mechanisms of inclusive heavy quark production can be classified as is shown in Fig. 13. The sum of this

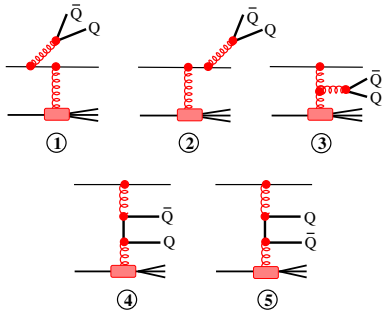

Figure 13: Feynman graphs contributing to inclusive production of a heavy quark pair.

five amplitudes can be assigned to two classes which we call bremsstrahlung (Br) and production (Pr) mechanisms, as is described in detail in [27],

$$\sum_{i=1}^{5} M_i = M_{Br} + M_{Pr} \,, \tag{14}$$

The bremsstrahlung amplitude, M_{Br}, corresponds to the following combination of graphs depicted in Fig. 13,

$$M_{Br} = M_1 + M_2 + \frac{Q^2}{M^2 + Q^2} M_3 \,. \tag{15}$$

It describes bremsstrahlung of a heavy gluon, which decays into $\bar{Q}Q$. The remaining amplitudes are combined into the second group, the amplitude of $\bar{Q}Q$ production via direct interaction with the heavy quark pair,

$$M_{Pr} = \frac{M^2}{M^2 + Q^2} M_3 + M_4 + M_5 \,. \tag{16}$$

The mechanisms of diffractive production are related to the inclusive ones by the Cutkosky cutting rules [28]. The second exchanged gluon in the Pomeron can be attached not only to the active quark radiating heavy flavours, but also to the spectator partons, separated by large distances. Diffraction excitation of $\bar{Q}Q$ in a separate parton by the bremsstrahlung mechanism, which is forbidden for DY process, is permitted for non-abelian radiation, but it is a higher twist effect and can be neglected. The presence of spectator partons in the projectile hadron opens new possibilities of interactions, and the bremsstrahlung mechanism becomes leading twist as well. Quantitatively, however, it is still a small part of the cross section. The dominant contribution comes from diffractive excitation of a separate projectile quark or gluon via the production mechanism.

The results of parameter-free calculations in the dipole approach agree well with available data from the Tevatron, as is demonstrated in Fig. 14. In particular,

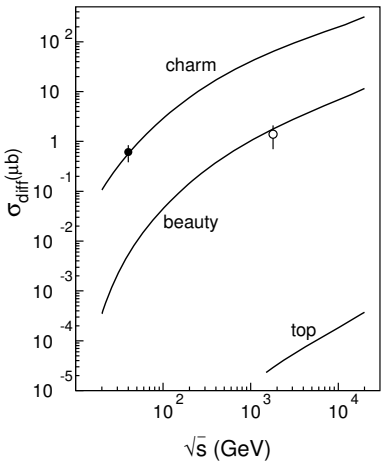

Figure 14: Cross section of diffractive production of heavy flavours as function of energy. Experimental points are from the E690 [29], and CDF [30] experiment.

the data confirm the leading twist behaviour of the cross section, $1/m_Q^2$, on the contrary to the higher twist, $1/m_Q^4$, suggested by diffractive factorisation.

8. Breakdown of QCD factorisation in diffraction

The graph in Fig. 5 suggests that diffractive DIS can be employed as a tool for measuring the structure func-

tion (PDFs) of the Pomeron [21]. Once the parton densities in the Pomeron are known and diffractive factorisation is at work, it is tempting to predict the cross section of any hard hadronic diffraction.

However, the attempts to use the diffractive PDFs of the Pomeron extracted from DIS to predict diffractive jet production failed badly: data from the Tevatron [31] contradict the predictions, based on HERA measurements, by an order of magnitude [32]. Factorisation

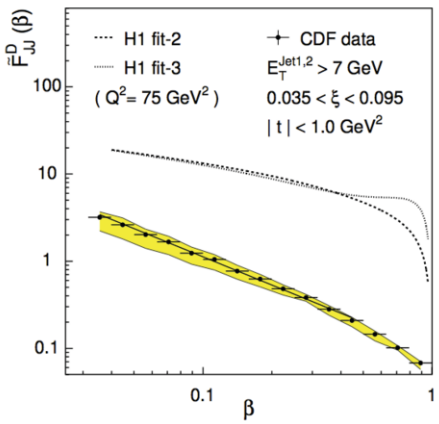

Figure 15: The dotted curves are the predictions made using the Pomeron PDFs extracted from diffractive DIS. Experimental points show the cross section of diffractive di-jet production [31, 32]

is severely broken for hard hadronic diffractions. This happens because of the impossibility to separate short and long distances in the hadronic diffractive interactions. The two scales mix up, and their interplay control the magnitude of the diffractive hadronic cross section.

Frequently the observed suppression is interpreted as the rapidity gap survival probability. That is of course a part of the mechanisms of factorisation breaking considered here, but it is oversimplified, because misses the leading twist and leaves diffraction to be a higher twist effect.

9. Diffractive Higgs production

Light quark do not radiate Higgs directly, because the coupling is too small. Higgs, however, can be produced in a double-step process: production of heavy quark, which then radiate a Higgs. Therefore, although Higgs is an Abelian particle, its radiation involves the non-Abelian mechanism of diffractive heavy quarks production.

Diffractive Higgsstrahlung is similar to diffractive DY, Z and W, since in all cases the radiated particle does not participate in the interaction. However, the Higgs

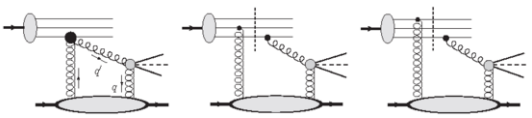

Figure 16: The dominat contributions to the diffractive Higgsstrahlung off heavy quarks.

decouples from light quarks, so the cross section of higgsstrahlung by light hadrons was found in [33] to be quite small.

A larger cross section emerges due to presence of intrinsic heavy flavours in light hadrons [34]. Exclusive Higgs production, $pp \to Hpp$, via coalescence of heavy quarks, $\bar{Q}Q \to H$. The contributions of different heavy flavours are compared in Fig. 17.

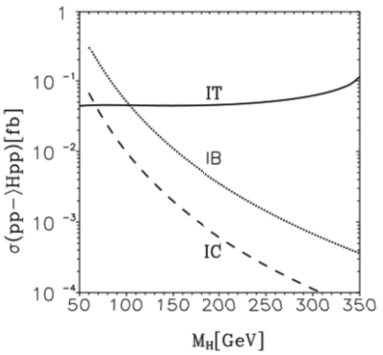

Figure 17: The cross section of $pp \to Hp+p$ as function of the Higgs mass. Contributions of IC (dashed) of IB (dotted) and IT (solid).

The cross section of Higgs production was evaluated assuming 1% of intrinsic charm, and that heavier flavours scale as $1/m_Q^2$ [35]. At the Higgs mass 125 GeV intrinsic bottom and top give comparable contributions.

10. Diffractive gluon radiation

The triple-Regge graphs, contributing to diffraction, have different quark-gluon structures. Fig. 19 represents the graph PPR corresponding to excitation of the valence quark skeleton. A hadron can be also excited

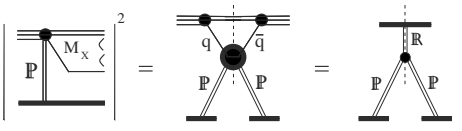

Figure 18: Diffraction due to excitation of the valence quark skeleton.

by radiation of a gluon, which would correspond to the triple Pomeron graph of Fig. 19.

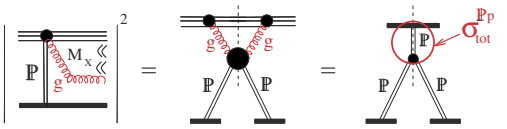

Figure 19: The triple-Pomeron graph originated from diffractive gluon radiation.

The two mechanisms can be discriminated by their M_X-dependences, which are quite different,

$$\left.\frac{d\sigma_{sd}}{dM_X^2}\right|_{PPR} \propto \frac{1}{M_X^3};$$
$$\left.\frac{d\sigma_{sd}}{dM_X^2}\right|_{PPP} \propto \frac{1}{M_X^2}.$$

Fitting data [36] one can extract from the analysis the Pomeron-proton cross section. Since the Pomeron is a gluonic object, it should interact stronger than a quark-antiquark meson, so one could anticipate $\sigma_{tot}^{Pp} \approx (9/4)\,\sigma_{tot}^{\pi p} \approx 50$ mb, however, the results of analyses presented in Fig. 20 show a much smaller value, $\sigma_{tot}^{Pp} \lesssim 2$ mb.

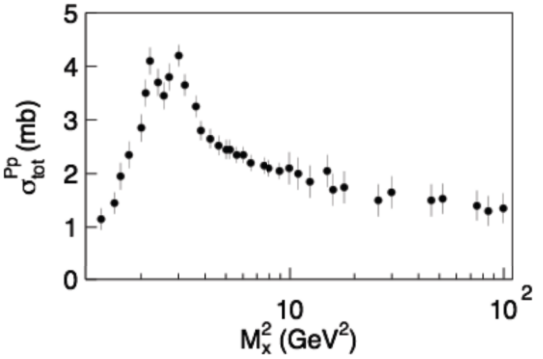

Figure 20: The Pomeron-proton cross section extracted from data on diffraction $pp \to pX$ [37]

The only solution for this puzzle is to assume that the Pomeron is a small size object, and its cross section is reduced due to colour transparency. This means that gluons in the proton have to be located within small spots of radius $r \approx 0.3$ fm [22, 38]

11. Nuclear shadowing

Interpretation of nuclear shadowing [39] depends on reference frame. Only observables must be Lorentz invariant. If the bound nucleons are well separated in the nuclear rest frame, after a Lorentz boost, both the nucleon size and the inter-nucleon spacings are Lorentz contracted, so the nucleons still seem to not "talk" to each other.

However, while the Lorentz contraction factor is m/E for the inter-nucleon spacing, it is weaker, $m/(xE)$, for partons, carrying fractional momentum x. Thus, the longitudinal propagation of small-x partons is larger. They overlap and start "talking" to each other, e.g. they can fuse and reduce the parton density at small x, as is illustrated in Fig. 21. Correspondingly, the cross section

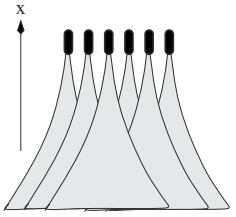

Figure 21: A cartoon of a Lorentz boosted and contracted nucleus. The horizontal and vertical axes are assumed to be longitudinal coordinate and Bjorken x.

decreases. This phenomenon is called shadowing, because in the rest frame of the nucleus the same process looks differently, as a reduction of the beam flux due to competition between different target nucleons. It is usually associated with the Glauber-Gribov mechanism of shadowing [40, 41], which is illustrated in Fig. 22.

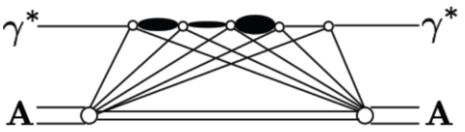

Figure 22: Grauber multiple-scattering shadowing, improved with the Gribov inelastic corrections, related to intermediate excitations of the projectile hadron.

The lowest order of the Gribov inelastic shadowing correction can be modelled as,

$$\Delta\sigma_{tot}^{\gamma^* A} = -4\pi \int d^2b\, e^{-\frac{1}{2}\,\sigma_{tot}^{hN} T_A(b)} \times \int_{M^2_{min}} dM^2 \frac{d\sigma_{sd}^{\gamma^* N}(p_T=0)}{dM^2\, dp_T^2} \int_{-\infty}^{\infty} dz_1 \rho_A(b,z_1) \times \int_{z_1}^{\infty} dz_2\, \rho_A(b,z_1)\, e^{iq_L(z_2-z_1)}, \qquad (17)$$

where $q_L = (M^2 + Q^2)/2E_{\gamma^*}$; $\rho_A(\vec{b},z)$ is the nuclear

density. The main problem for this kind of calculations comes from the unknown absorption cross section $\sigma_{tot}^{h^*N}$, which is fixed here at σ_{tot}^{hN}. Also the transitions between different excited states are unknown and neglected.

Nearly Q^2 independent $\sigma_{diff}^{DIS}/\sigma_{incl}^{DIS}$ leads to a weak Q^2 dependence of nuclear shadowing. Different triple-Reggeon terms in diffraction correspond to different parts of the shadowing effect: the PPR and PPP terms give quark and gluon shadowing respectively.

The onset of shadowing is controlled by the coherence length, which can be interpreted as the $\bar{q}q$ fluctuation lifetime assuming that is is moving with the speed of light.

$$l_c = \frac{1}{q_L} = \frac{P}{x_{Bj}\, m_N} = P\, l_c^{max}. \tag{18}$$

At $l_c \ll R_A$ there is no shadowing, but at $l_c \gg R_A$ the dipole size is frozen and the calculations are much simplified,

$$\left(\sigma_{tot}^{\gamma^* A}\right)_{l_c \gg R_A}^{T,L} = 2 \int d\alpha \int d^2 r \left|\Psi_{\bar{q}q}^{T,L}(\varepsilon r)\right|^2 \times \int d^2 b \left[1 - \exp\left(-\frac{\sigma_{q\bar{q}}^N(r)}{2} T(b)\right)\right]. \tag{19}$$

The mean coherence length for a $\bar{q}q$ fluctuation in vacuum vanishes [42],

$$\langle P \rangle_{vac} = \frac{\left\langle \Psi_{\bar{q}q}^{\gamma^*} \middle| P(k_T, \alpha) \middle| \Psi_{\bar{q}q}^{\gamma^*} \right\rangle}{\left\langle \Psi_{\bar{q}q}^{\gamma^*} \middle| \Psi_{\bar{q}q}^{\gamma^*} \right\rangle} \to 0. \tag{20}$$

However, the vacuum fluctuations are dominated by heavy, small size pairs, most of which cannot interact. For those fluctuations, which do participate in the interaction,

$$\langle P \rangle_{shad} = \frac{\left\langle f(\gamma^* \to \bar{q}q) \middle| P(k_T, \alpha) \middle| f(\gamma^* \to \bar{q}q) \right\rangle}{\left\langle f(\gamma^* \to \bar{q}q) \middle| f(\gamma^* \to \bar{q}q) \right\rangle}. \tag{21}$$

In real data the photon fluctuations in DIS are not frozen, but keep breathing during propagation through the nucleus. The dipole breathing can be calculated with the path-integral technique [22, 42].

The coherence length for gluons is quite shorter than for quarks, because gluons, located in small spots, have larger transverse momentum, so gluonic fluctuations are heavier. Relative shortness of the gluon coherence time is a good support for factorisation of the dipole interaction.

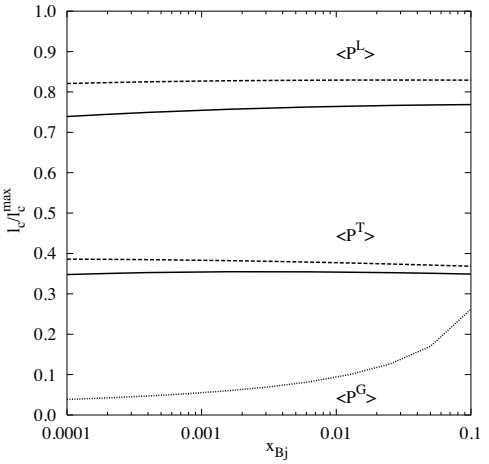

Figure 23: The mean values of factor $P^{T,L}$ in Eq. (18), controlling the coherence length, as function of Bjorken x_{Bj}. Solid and dashed curves correspond to $Q^2 = 4$ and $40\,\mathrm{GeV}^2$.

There are many evidences for the two-scale structure of hadrons [38], which leads to a weak gluon shadowing. A DGLAP analyses is able to single out from data the nuclear PDFs for different species of partons. A leading order analysis [43] failed to extract the gluon distribution from the NMC data, but the NLO fit turned out to be sensitive to gluons. The results of the NLO analysis in Ref. [44] presented in Fig. 24 confirm a very weak, gluon shadowing.

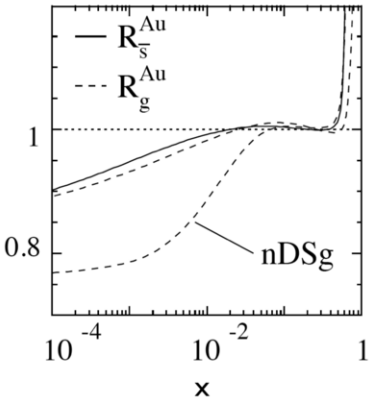

Figure 24: The result of the NLO global analysis [44] for the nuclear ratio Au/p for gluons vs Bjorken x at $Q^2 = 10\,\mathrm{GeV}^2$. Gluons are plotted by dashed curve. The curve marked as nDSg is a trial function with bad value of χ^2 testing the stability of the analysis.

The first tests of gluon shadowing at LHC, well confirmed the anticipated weakness of gluon shadowing. Namely the magnitude of the Cronin ratio A/p for high-p_T pion production in pA collisions was correctly

predicted in [45], prior the RHIC and LHC data, to exceed unity by few percent. Both predictions were well confirmed [46, 47], while numerous recent calculations presented in [48] overestimated the strength of gluon shadowing and under-predicted the nuclear ratio.

12. Summary

Factorisation of long-distance soft and short-distance hard interactions is expected to be valid for inclusive reactions (except some specific kinematic regions), is demonstrated to fail for diffractive processes, which are dominated by the strong interplay between soft and hard interactions. This was demonstrated above for several examples of diffractive reactions, Drell-Yan reaction, production of gauge bosons and Higgs, production of heavy flavours. All processes were treated in the dipole representation, which explicitly discriminates between the short and long transverse distances. Factorisation is also broken in inclusive hard reactions on nuclei, where quark shadowing (higher twist) and the hard process are controlled by the same parameter, the dipole size.

Acknowledgements: I am thankful to the organisers of the 10th SILAFAE, inviting me to deliver this talk, for kind hospitality and a partial support. This work was partially supported by Fondecyt (Chile) grant 1130543, and by the ECOS grant C12E04.

References

[1] J. C. Collins, D. E. Soper and G. F. Sterman, Adv. Ser. Direct. High Energy Phys. **5** (1988) 1.
[2] V. N. Gribov and L. N. Lipatov, Sov. J. Nucl. Phys. **15** (1972) 438.
[3] L. N. Lipatov, Sov. J. Nucl. Phys. **20** (1975) 95.
[4] G. Altarelli and G. Parisi, Nucl. Phys. **B126** (1977) 298.
[5] Yu. L. Dokshitzer, Sov. Phys. JETP **46** (1977) 641.
[6] K.A. Olive et al. (Particle Data Group), Chin. Phys. C **38** (2014) 090001.
[7] S. D. Drell and T. M. Yan, Phys. Rev. Lett. **25** (1970) 316 [Erratum-ibid. **25** (1970) 902].
[8] J. Raufeisen, J. C. Peng and G. C. Nayak, Phys. Rev. D **66** (2002) 034024.
[9] B. Z. Kopeliovich, L. I. Lapidus and A. B. Zamolodchikov, JETP Lett. **33** (1981) 595 [Pisma Zh. Eksp. Teor. Fiz. **33** (1981) 612].
[10] N. N. Nikolaev and B. G. Zakharov, Z. Phys. **C49** (1991) 607.
[11] J. B. Kogut and D. E. Soper, Phys. Rev. **D1** (1970) 2901.
[12] J. M. Bjorken, J. B. Kogut, and D. E. Soper, Phys. Rev. **D3** (1971) 1382.
[13] B. Z. Kopeliovich, I. K. Potashnikova and I. Schmidt, Braz. J. Phys. **37** (2007) 473.
[14] B. Kopeliovich and B. Povh, Z. Phys. A **356** (1997) 467.
[15] B. Z. Kopeliovich, proc. of the workshop Hirschegg '95: Dynamical Properties of Hadrons in Nuclear Matter, Hirschegg January 16-21, 1995, ed. by H. Feldmeyer and W. Nörenberg, Darmstadt, 1995, p. 102 (hep-ph/9609385).
[16] S. J. Brodsky, A. Hebecker, and E. Quack, Phys. Rev. D**55** (1997) 2584.
[17] B. Z. Kopeliovich, J. Raufeisen, A. V. Tarasov, Phys. Lett. **B503** (2001) 91
[18] R. J. Glauber, Phys. Rev. 100, 242 (1955).
[19] E. Feinberg and I. Ya. Pomeranchuk, Nuovo. Cimento. Suppl. 3 (1956) 652.
[20] M. L. Good and W. D. Walker, Phys. Rev. 120 (1960) 1857.
[21] G. Ingelman, P. E. Schlein, Phys. Lett. **B152** (1985) 256.
[22] B. Z. Kopeliovich, A. Schäfer and A. V. Tarasov, Phys. Rev. **D62** (2000) 054022.
[23] B. Z. Kopeliovich, I. K. Potashnikova, I. Schmidt, A. V. Tarasov, Phys. Rev. **D74** (2006) 114024.
[24] R. S. Pasechnik and B. Z. Kopeliovich, Eur. Phys. J. C **71** (2011) 1827.
[25] R. Pasechnik, B. Kopeliovich and I. Potashnikova, Phys. Rev. D **86** (2012) 114039.
[26] T. Aaltonen *et al.* [CDF Collaboration], Phys. Rev. D **82** (2010) 112004.
[27] B. Z. Kopeliovich, I. K. Potashnikova, I. Schmidt and A. V. Tarasov, Phys. Rev. D **76** (2007) 034019.
[28] R.E. Cutkosky, J. Math. Phys. 1 (1960) 429.
[29] M.H.L.S. Wang et al. [E690 Collaboration], Phys. Rev. Lett. **87** (2001) 082002.
[30] T. Affolder et al. [CDF Collaboration], Phys. Rev. Lett, **84**, (2000).
[31] T. Affolder *et al.* [CDF Collaboration], Phys. Rev. Lett. **84** (2000) 5043.
[32] K. Goulianos, Proceedings of the 13th International Conference on Elastic and Diffractive Scattering, CERN, Geneva, (2009) 121.
[33] R. Pasechnik, B. Z. Kopeliovich and I. K. Potashnikova, arXiv:1403.2014 [hep-ph].
[34] S. J. Brodsky, B. Kopeliovich, I. Schmidt and J. Soffer, Phys. Rev. D **73** (2006) 113005.
[35] M. Franz, V. Polyakov and K. Goeke, Phys. Rev. D **62**, 074024 (2000).
[36] Y. M. Kazarinov, B. Z. Kopeliovich, L. I. Lapidus and I. K. Potashnikova, Sov. Phys. JETP **43** (1976) 598 [Zh. Eksp. Teor. Fiz. **70** (1976) 1152].
[37] A.B. Kaidalov, Phys. Rept. **50** (1979) 157.
[38] B. Z. Kopeliovich, I. K. Potashnikova, B. Povh and I. Schmidt, Phys. Rev. D **76** (2007) 094020.
[39] B. Z. Kopeliovich, J. G. Morfin and I. Schmidt, Prog. Part. Nucl. Phys. **68** (2013) 314.
[40] R. J. Glauber, in *Lectures in Theoretical Physics*, Editors: W. E. Brittin *et al.* (New York, 1959).
[41] V. N. Gribov, Sov. Phys. JETP **29** (1969) 483 [Zh. Eksp. Teor. Fiz. **56** (1969) 892].
[42] B. Z. Kopeliovich, J. Raufeisen and A. V. Tarasov, Phys. Rev. C **62** (2000) 035204.
[43] K. J. Eskola, V. J. Kolhinen and P. V. Ruuskanen, Nucl. Phys. B **535** (1998) 351; K. J. Eskola, V. J. Kolhinen and C. A. Salgado, Eur. Phys. J. C **9** (1999) 61.
[44] D. de Florian and R. Sassot, Phys. Rev. D **69** (2004) 074028.
[45] B. Z. Kopeliovich, J. Nemchik, A. Schafer, A. V. Tarasov, Phys. Rev. Lett. **88** (2002) 232303.
[46] B. Z. Kopeliovich, J. Nemchik, I. K. Potashnikova and I. Schmidt, Int. J. Mod. Phys. E **23** (2014) 4, 1430006.
[47] B. Z. Kopeliovich and J. Nemchik, J. Phys. G **38** (2011) 043101.
[48] J. L. Albacete, N. Armesto, R. Baier, G. G. Barnafoldi, J. Barrette, S. De, W.-T. Deng and A. Dumitru *et al.*, Int. J. Mod. Phys. E **22** (2013) 1330007.